INFORMATION TO USERS

This manuscript has been reproduced from the microfilm master. UMI films the text directly from the original or copy submitted. Thus, some thesis and dissertation copies are in typewriter face, while others may be from any type of computer printer.

The quality of this reproduction is dependent upon the quality of the copy submitted. Broken or indistinct print, colored or poor quality illustrations and photographs, print bleedthrough, substandard margins, and improper alignment can adversely affect reproduction.

In the unlikely event that the author did not send UMI a complete manuscript and there are missing pages, these will be noted. Also, if unauthorized copyright material had to be removed, a note will indicate the deletion.

Oversize materials (e.g., maps, drawings, charts) are reproduced by sectioning the original, beginning at the upper left-hand corner and continuing from left to right in equal sections with small overlaps. Each original is also photographed in one exposure and is included in reduced form at the back of the book.

Photographs included in the original manuscript have been reproduced xerographically in this copy. Higher quality 6" x 9" black and white photographic prints are available for any photographs or illustrations appearing in this copy for an additional charge. Contact UMI directly to order.

UMI

A Bell & Howell Information Company
300 North Zeeb Road, Ann Arbor MI 48106-1346 USA
313/761-4700 800/521-0600

RICE UNIVERSITY

A CYCLOADDITION-BASED FULLERENE ASSEMBLY MECHANISM

by

DOUGLAS STROUT

A THESIS SUBMITTED
IN PARTIAL FULFILLMENT OF THE
REQUIREMENTS FOR THE DEGREE
DOCTOR OF PHILOSOPHY

APPROVED, THESIS COMMITTEE

G E Scuseria

Gustavo E. Scuseria, Professor, Director
Chemistry

R. E. Smalley

Richard E. Smalley, Professor
Chemistry and Physics

Walter Chapman

Walter Chapman, Assistant Professor
Chemical Engineering

Houston, Texas

September 1995

ABSTRACT

A Cycloaddition-based Fullerene Assembly Mechanism

by

Douglas Strout

Since their discovery, the fullerenes have challenged scientists with a wide array of problems concerning their properties, behavior and potential applications. One such fundamental question is that of the assembly of these carbon cages. Much effort has been directed at obtaining an understanding of the process whereby graphite is transformed into fullerenes. In this work, a theoretical study is carried out to explore the nature of carbon clusters, including the fullerenes themselves as well as other structures which may be intermediates along the path to fullerenes. The experiments which generate fullerenes are interpreted by the use of theoretical calculations, and this interpretation is used to develop a model for a fullerene assembly pathway.

The principal tenets of the model are as follows: 1) The process of forming fullerenes is begun by the cycloaddition of monocyclic carbon rings, 2) The cycloadducts, once formed, undergo unimolecular reactions to form cylindrical carbon "hoops", 3) Closed cages can form from "hoops" through a sequence of 1,2-carbon shifts and cyclization reactions, and 4) The cages can "anneal" to find the most stable isomer by rearranging their bonds. Energetics of the reactions involved in each step of the model will be explored computationally by the Hartree-Fock method and several electron correlation methods. Energetic details will include both overall reaction energetics and transition barriers for the reactions. The computational results will be shown to be consistent with experimental results, so that a reasonable synthesis of theory and experiment can be presented.

ACKNOWLEDGMENTS

Dr. Gustavo Scuseria is acknowledged for the contribution of his experience, expertise, and patience to the development of this work. Gregory Odom, Lewis Book, John Millam, and Dr. Chunhui Xu are acknowledged for their contributions to the methods and programs that were employed in this work. Robert Murry is acknowledged for his contribution to the work concerning the annealing and fragmentation of fullerenes.

Patricia Strout is acknowledged for support of this work in many intangible yet essential ways.

I acknowledge my Lord Jesus Christ for bringing me through the triumphs and trials that led to the completion of this work.

Table of Contents

LIST OF TABLES

LIST OF FIGURES

Chapter 1

Introduction

In 1985, the discovery[1] of buckminsterfullerene (BF) prompted a flurry of activity as scientists sought to characterize this new form of carbon and produce it in bulk quantities. When bulk synthesis[2] was achieved in 1990, scientific investigation of buckminsterfullerene intensified and diversified as various research groups produced a wide array of both endohedral and exohedral derivatives. C_{70}, C_{76}, C_{78} and still larger fullerenes have been isolated.[3] Furthermore, other fullerene-like forms such as "buckytubes"[4] (long, cylindrical graphitic objects) and "buckyonions"[5] (fullerenes within fullerenes) have been created in the laboratory. A vast array of hypothetical applications have been investigated, ranging from the synthesis of carbon-based superconductors[6] to the creation of fullerene derivatives to combat AIDS.[7]

A fundamental question about C_{60} and the other fullerenes is the mechanism of their formation. What happens to graphite after it is vaporized which leads to the appearance of carbon cages? Various models have been

---

[1]H.W. Kroto, J.R. Heath, S.C. O'Brien, R.F. Curl, and R.E. Smalley. *Nature* **318**, 162 (1985).
[2]W. Krätschmer, L.D. Lamb, K. Fostiropoulos, and D.R. Huffman. *Nature* **347**, 354 (1990).
[3]F. Diederich and R.L. Whetten. *Acc. Chem. Res.* **25**, 119 (1992).
[4]S. Iijima. *Nature* **354**, 56 (1991).
[5]D. Ugarte. *Nature* **359**, 707 (1992).
[6]Y.H. Kao et al. *Solid State Communications* **87**, 387 (1993).
J. Travis. *Science* **261**, 1392 (1993).
[7]F. Wudl, R. Sijbesma, G. Srdanov, C.L. Wilkins, and J.A. Castoro. *J. Am. Chem. Soc.* **115**, 6510 (1993).
S.H. Friedman, G.L. Kenyon, and D.L. DeCamp. *J. Am. Chem. Soc.* **115**, 6506 (1993).

advanced. The "pentagon road" model[8] suggests that fullerenes form from the successive addition of small carbon species to the edges of curved graphitic precursors until cage closure results. The "fullerene road"[9] advances the idea that carbon cages of all sizes are formed in the experiments but then add or lose C_2 radicals until a 60-atom cage is formed. Also, "ring stacking" models[10] exist which propose that C_{60} and the larger fullerenes are formed by the sequential addition of specific carbon rings.

A range of experiments have been conducted to elucidate the formation of fullerenes. Ebbesen *et al.*[11] generated fullerenes by the resistive heating of two graphite rods with different abundances of carbon-13. The purpose of the experiments was to determine the form in which graphite is removed from the surface of the rods. For example, if graphite were removed from the rods in sections large enough to close and form C_{60} independently, the mass spectrum of the C_{60} products should show two distinct mass distributions corresponding to the isotope ratios of the two rods. However, this was not observed. The C_{60} products showed mass distributions that indicated thorough isotopic mixing. This demonstrated that graphite is converted to an atomic carbon vapor before fullerenes are formed.

In another experiment, McElvany *et al.*[12] generated fullerenes from carbon rings produced by the laser desorption of organic precursors. C_{18}, C_{24}, and C_{30} were each used in a separate experiment. In each case, the mass spectra of the products showed peaks at integer multiples of the mass of the initial carbon ring.

---

[8]R.E. Smalley. *Acc. Chem. Res.* **25**, 98 (1992).
[9]J.R. Heath. *Fullerenes: Synthesis of C_{60} from small carbon clusters* (G.S. Hammond and V.J. Kuck, eds.) Washington, DC: American Chemical Society, 1992.
[10]T. Wakabayashi and Y. Achiba. *Chem. Phys. Lett.* **190**, 465 (1992).
[11]T.W. Ebbesen, J. Tabuchi, and K. Tanigaki. *Chem. Phys. Lett.* **191**, 336 (1992).
[12]S.W. McElvany, M.M. Ross, N.S. Goroff, and F. Diederich. *Science* **259**, 1594 (1993).

The C_{30} experiment showed an enormous peak at C_{60}, owing to the special stability of buckminsterfullerene, and much smaller peaks at C_{90}, C_{120}, etc. C_{18} and C_{24} both produced large C_{70} peaks, because both can form C_{72}, which then dissociates C_2 to give the stable C_{70}. These experiments demonstrated that carbon rings can be converted to fullerenes, but does a rings-to-fullerenes assembly pathway have any application when graphite is the starting material?

Recently, a powerful tool has been introduced for examining the details of graphite vaporization experiments. An experimental technique, known as "ion chromatography,"[13] has revealed new insights into the fullerene formation experiments. With this technique, the cluster ions produced by graphite vaporization are mass-selected and injected into a tube that is filled with an inert gas, usually helium. The ions move through the length of the tube, and collisions between the clusters and the inert gas cause the clusters to be separated by cross-section, as the more compact clusters exit the tube at earlier times. The resulting plot of cluster intensity versus time is called an "arrival time distribution" (or ATD).

von Helden *et al.*[14] performed ion chromatography on the graphite vaporization products and reported several peaks in the ATD. For carbon clusters with 10-20 atoms, a single peak appeared. Beginning with C_{21}, two peaks were observed, and for 30 or more atoms, three more peaks were seen, for a total of five. An ATD for C_{36}, showing all five peaks, is displayed in Figure 1. Those authors also developed a method for assigning the arrival time peaks to structural cluster isomers. For each proposed structural isomer, they optimized the geometry using the semiempirical PM3 method. Each optimized

---

[13]P.R. Kemper and M.T. Bowers. *J. Am. Soc. Mass Spectrom.* **1**, 197 (1990).
P.R. Kemper and M.T. Bowers. *J. Phys. Chem.* **95**, 5134 (1991).
[14]G. von Helden, M.-T. Hsu, N. Gotts, and M.T. Bowers. *J. Phys. Chem.* **97**, 8182 (1993).

geometry was then used for a Monte Carlo simulation of the collisions between the proposed cluster and the helium atoms. This procedure yields a theoretical cross-section for the cluster, which is then converted to a convenient scale called the "mobility" scale. The experimental arrival times are also converted to mobilities, and if a match is obtained, the proposed cluster is assigned to the experimental peak.

According to the von Helden *et al.* model, the peak that is seen beginning at C_{10} corresponds to a monocyclic carbon ring and is called the "Ring I" peak. The second peak observed at C_{21} is denoted the "Ring II" peak and is matched to planar bicyclic rings. One of the three peaks appearing at C_{30} is named "Ring III" and is interpreted as planar tricyclic structures. Another peak is of very low intensity and has been dubbed "3-D ring." The interpretation of the 3-D ring peak was not clearly made, although graphitic sheets were suggested as a possibility. The final peak, corresponding to the most compact structures observed in the experiment, is assigned to fullerenes. Examples of 36-atom clusters of each type are shown in Figure 2.

Following the method of von Helden *et al.*, Book *et al.*[15] developed a mobility code and used the code to illustrate two important points about the theoretical mobilities. First, calculated mobilities were shown to be insensitive to molecular vibration. This validates the use of static, equilibrium geometries for the mobility calculations. Also, these mobilities were shown to be insensitive to the choice of the level of theory employed when obtaining optimized geometries. Therefore, fast, semiempirical methods can be used to obtain valid geometries quickly.

---

[15]L.D. Book, C.H. Xu, and G.E. Scuseria. *Chem. Phys. Lett.* **222**, 281 (1994).

The ion chromatography method of interpreting graphite vaporization experiments has power because it reveals information about clusters that are produced in the process that ultimately leads to fullerenes. In fact, some of the other structures which appear in this experiment may be intermediates in the formation of fullerenes, and understanding the nature of those intermediates sheds light on the fullerene formation mechanism itself. However, mobility calculations can only demonstrate that a proposed cluster is consistent with experimental observation. The identification of a cluster by its mobility is not definitive, and that uncertainty is where the work of this thesis begins.

Figure 1

Arrival time distribution for C_{36}. Reprinted with permission from G. von Helden, M.T.-Hsu, N. Gotts, and M.T. Bowers. *J. Phys. Chem.* **97**, 8182 (1993). Copyright 1993 American Chemical Society

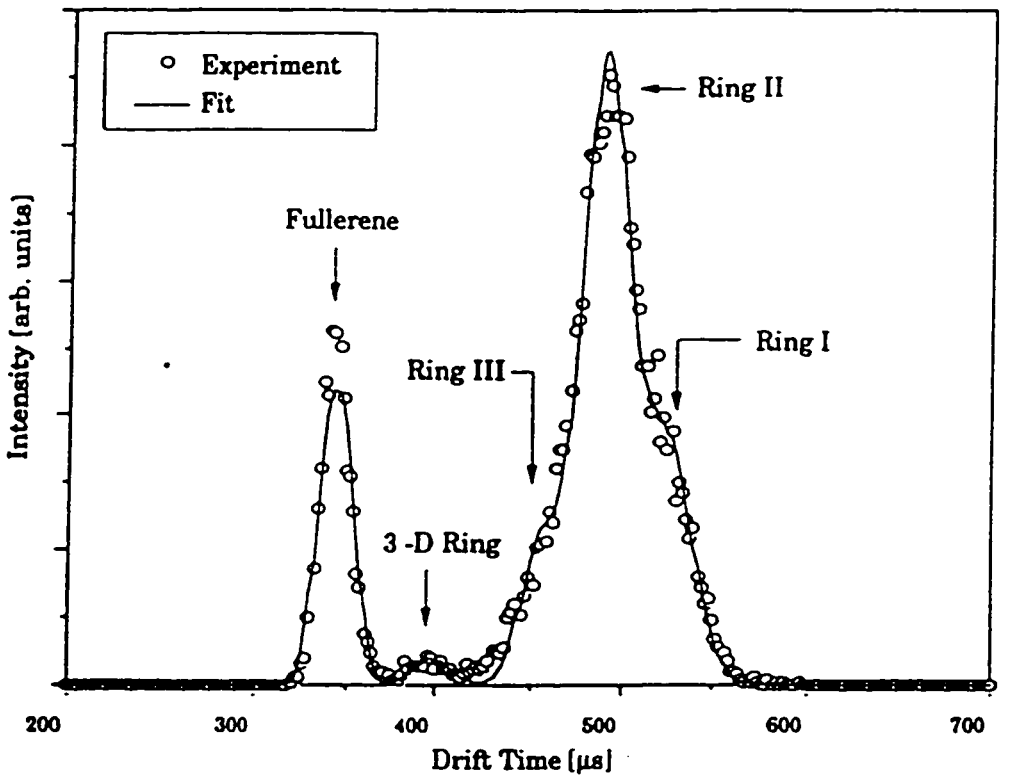

Figure 2

C_{36} structures corresponding to the five peaks in the ATD, according to the von Helden et al. model
(a) Ring I (b) Ring II (c) Ring III (d) 3-D ring (e) Fullerene

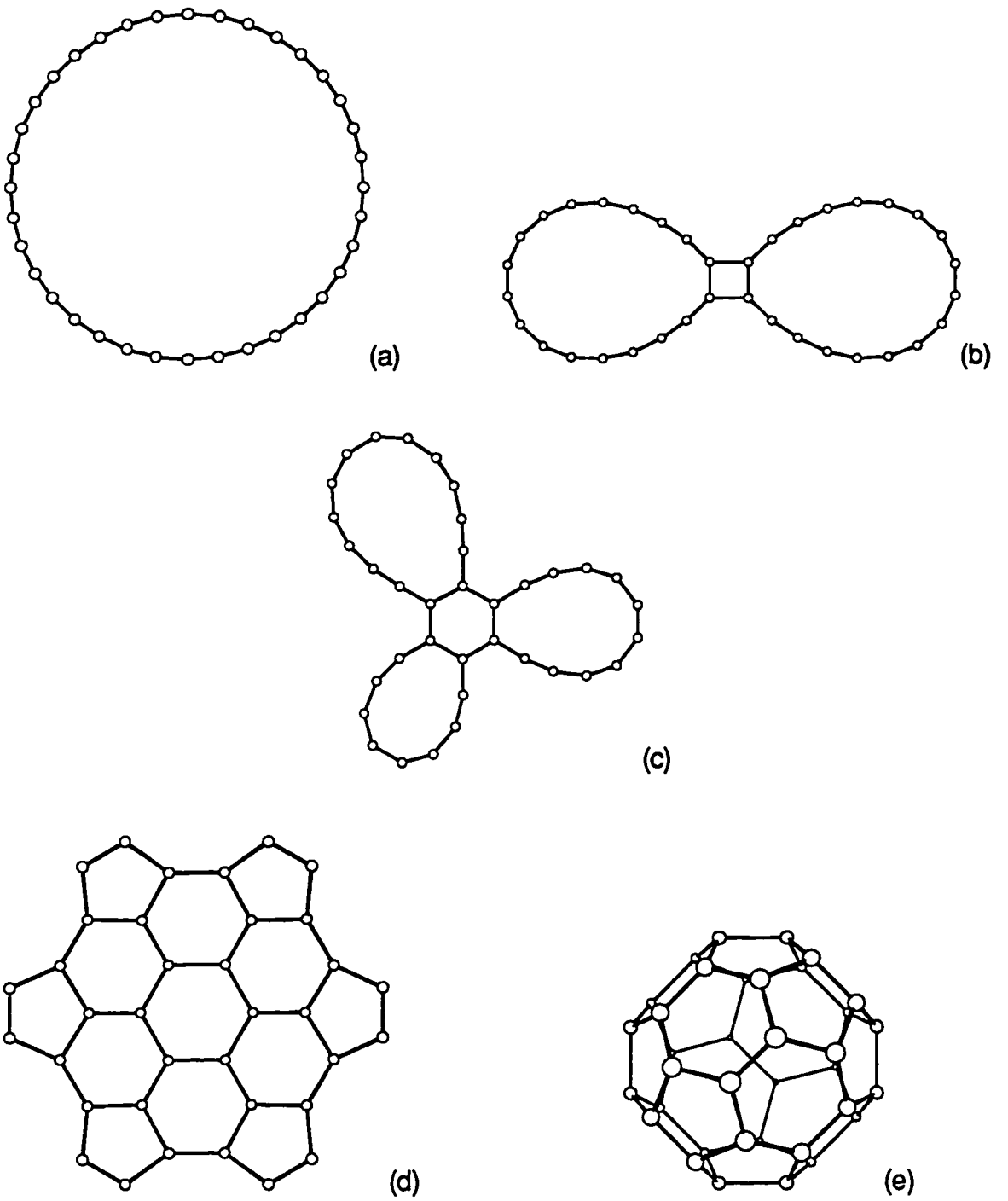

Chapter 2

The Cycloaddition Model

In the present work, a new interpretation[16] of the ion chromatography experiments has been developed using the Book *et al.*[15] mobility code. Quantitative mobility data has been computed for clusters with 36, 40, 44, and 48 carbon atoms. This range of cluster sizes is selected because, for smaller clusters, some of the five arrival time peaks are absent and, for larger clusters, the experimental resolution between the "Ring" peaks becomes very poor. Optimized geometries are obtained using a semiempirical tight-binding (TB) carbon-carbon potential,[17] which has been successful in previous carbon-based applications.[18]

Mobility data for the monocyclic rings is shown in Table 1. Over the range of cluster sizes studied, calculated mobilities for monocyclic rings consistently match Ring I experimental results. Also, the most stable fullerene isomer[19] at each cluster size matches the results for the peak in the ATD previously assigned to fullerenes. Data for the fullerenes is also shown in Table 1. These results

---

[16]An introduction to the cycloaddition model is given in D.L. Strout, L.D. Book, J.M. Millam, C.H. Xu, and G.E. Scuseria. *J. Phys. Chem.* **98**, 8622 (1994).

[17]C.H. Xu, C.Z. Wang, C.T. Chan and K.M. Ho. *J. Phys. Condens. Matter* **4**, 6047 (1992).

[18]D.L. Strout, R.L. Murry, C.H. Xu, W.C. Eckhoff, G.K. Odom, and G.E. Scuseria. *Chem. Phys. Lett.* **214**, 357 (1993); C.H. Xu and G.E. Scuseria. *Phys. Rev. Lett.* **72**, 669 (1994); B.L. Zhang, C.Z. Wang, K.M. Ho, C.H. Xu, and C.T. Chan. *J. Chem. Phys.* **97**, 5007 (1992); C.Z. Wang, C.H. Xu, C.T. Chan, and K.M. Ho. *J. Phys. Chem.* **96**, 3653 (1992).

[19]B.L. Zhang, C.Z. Wang, K.M. Ho, C.H. Xu, and C.T. Chan. *J. Chem. Phys.* **97**, 5007 (1992)

simply reproduce the previous work[14] and can be viewed as a useful benchmark for the mobility code.

Moreover, several graphitic sheets at each cluster size can be shown to have mobilities consistent with 3-D ring results, thereby establishing graphitic sheets as good candidates for 3-D ring clusters. The graphitic sheets are pictured in Figure 3, and the mobility data is shown in Table 2. Note that many of the graphitic sheets contain pentagons. Sheets with pentagons have 3-D ring mobilities, but only if the pentagons are on the perimeter of the sheet. Interior pentagons impart significant curvature to a graphitic sheet, which makes it too compact to have a 3-D ring mobility.

The Ring II peaks are matched by 2+2 cycloadducts of monocyclic rings; several cycloadducts are shown in Figure 4. Mobility data for 2+2 cycloadducts are presented in Table 3. The use of 2+2 cycloadducts follows the concept of the planar bicyclic ring from previous work, but it raises important questions about the kinds of reactions that might be taking place in the graphite vaporization experiments. For example, two 18-membered carbon rings can collide to form a 2+2 cycloadduct with 36 atoms, which is a species that is consistent with experimental observation. Since monocyclic carbon rings are the only molecules present in the size range 10-20 atoms, such reactions between rings may play an important role in the fullerene assembly process.

This idea is the centerpiece of the cycloaddition model for interpreting the ion chromatography results. Since 2+2 cycloaddition is experimentally consistent, other cycloadducts are proposed as candidates for experimentally observed isomers. The first reaction considered is 2+4 cycloaddition. Mobility data for TB optimized 2+4 cycloadducts is presented in Table 4 and demonstrates that the 2+4 cycloadducts are completely consistent with Ring III

experimental mobilities. Several 2+4 adducts are pictured in Figure 5. Note that the two rings which compose each adduct are not coplanar. This nonplanarity makes 2+4 adducts significantly more compact than the 2+2 adducts, hence the higher mobilities. The emergence of 2+4 cycloadducts as Ring III candidates provides support for the cycloaddition model and refutes previous arguments[14] that all of the "Ring" isomers were necessarily planar.

The next cycloaddition candidate is the 4+4 process. Since Tables 3 and 4 demonstrate that the mobilities of [a+b] cycloadducts with a given total number of atoms are insensitive to the precise sizes of the individual rings, only one 4+4 adduct will be selected at each cluster size. 4+4 mobilities are shown in Table 5, alongside 2+2 mobilities and Ring II results. For C_{36}, the 4+4 mobility is not close to Ring II, but for C_{48}, it is a good match. The reason for this is the difference in ring strain imposed by 2+2 versus 4+4 cycloaddition. For large rings, which can easily redistribute strain, 2+2 and 4+4 cycloaddition have virtually the same effect on the rings, hence roughly equal mobilities for the cycloadducts. Conversely, 4+4 distorts small rings more than does 2+2; in fact, 4+4 adducts for small rings are not even planar, as illustrated in Figure 6. This causes 4+4 mobilities to diverge wildly from Ring II and 2+2 mobilities for clusters with less than 40 atoms. Therefore, 4+4 cycloaddition is not a likely source of Ring II clusters.

Since it is clear that not all cycloadditions produce experimentally consistent isomers, it must be determined exactly which processes are consistent with experiment and whether, or if, a pattern exists to separate likely reactions from unlikely ones. Mobilities have been computed for 4+6 cycloadducts and tabulated in Table 6. This data reveals that the 4+6 adducts are, like the 2+4 adducts, consistent with Ring III experimental mobilities. Several 4+6

cycloadducts are pictured in Figure 7. The cycloaddition model yields two possibilities for Ring III in the graphite vaporization experiments. From a mobility standpoint, the 2+4 and 4+6 cycloadducts are totally indistinguishable. The Ring III arrival time peak may be the result of both 2+4 and 4+6 cycloadducts being present.

2+4 and 4+6 cycloaddition have the common characteristic that both are symmetry-allowed in the singlet state under the Woodward-Hoffmann rules. 2+2 cycloaddition, on the other hand, requires that one of the reactants be in the triplet state. It could be the case that 2+2 cycloaddition is the only reaction undergone by rings in the triplet state, whereas collisions between two rings in the singlet state result in a variety of reactions. It is interesting to note that von Helden *et al.* reported a "Ring IV" for C_{40}, and there exists a C_{40} 6+8 cycloadduct with the corresponding mobility (about 3.50 cm^2/volt second).

The cycloaddition model provides a consistent, plausible alternative to previous ion chromatography interpretations. Bimolecular reactions between monocyclic carbon rings can effectively explain all of the "Ring" isomers in the graphite vaporization experiments. However, as with the von Helden *et al.* model, the cycloaddition model based on cluster mobilities cannot stand alone because the structure identifications are not definitive. Stronger evidence is required.

Table 1

Comparison of theoretical (ref. 16) and experimental (ref. 14) mobilities for monocyclic carbon rings and fullerenes

(mobilities in cm^2/ volt second)

Cluster size	Ring I (exp)	Monocyclic (calc)	Fullerene (exp)	Fullerene (calc)
C_{36}	3.01	2.89	5.93	6.00
C_{40}	2.70	2.57	5.49	5.68
C_{44}	2.5	2.32	5.23	5.38
C_{48}	2.2	2.17	5.18	5.13

Figure 3

Graphitic sheets with 36-48 atoms

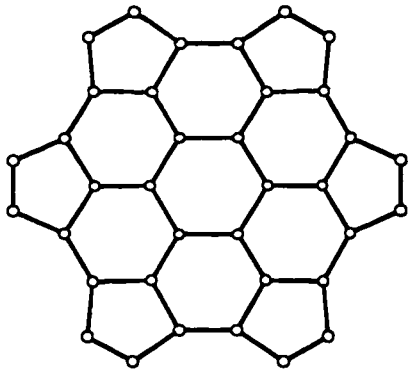

(36a)

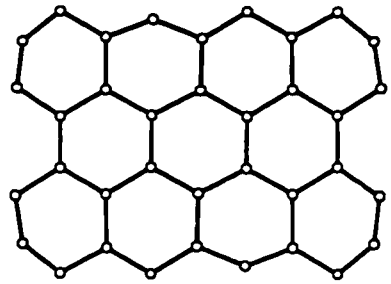

(36b)

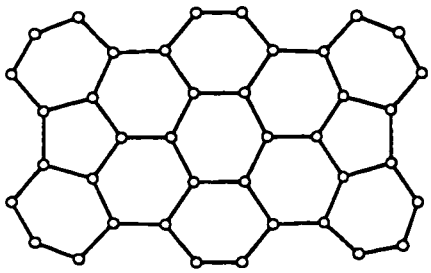

(40a)

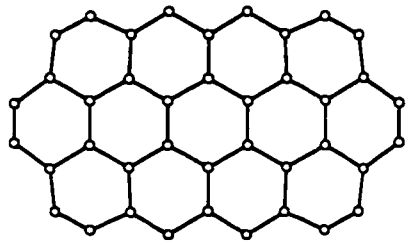

(40b)

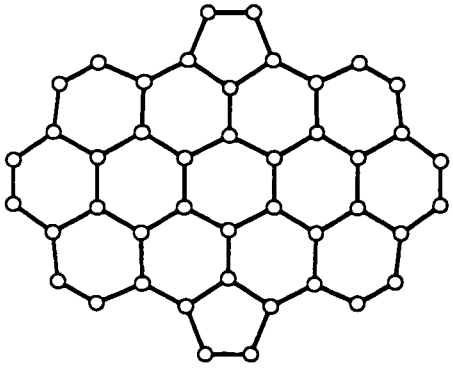

(44a)

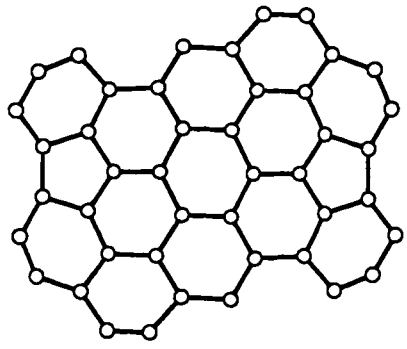

(44b)

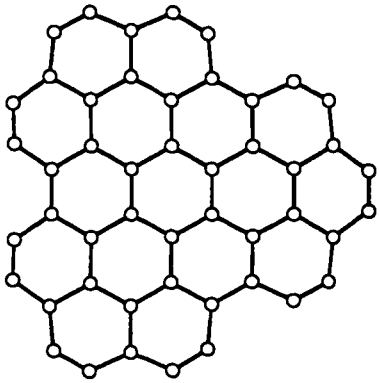

(48a)

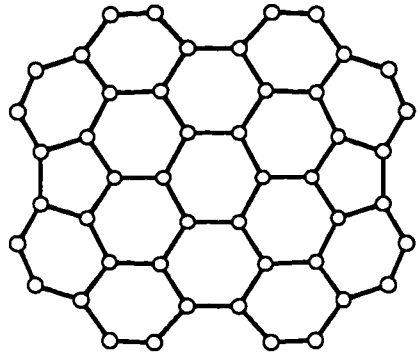

(48b)

Table 2

Mobilities of graphitic sheets compared to "3-D Ring" mobilities

(mobilities in cm^2/volt second)

Cluster size	3-D Ring mobility	Graphitic sheet	Mobility (calc)
C_{36}	4.58	36a	4.48
		36b	4.58
C_{40}	4.19	40a	4.19
		40b	4.18
C_{44}	4.0	44a	3.92
		44b	3.94
C_{48}	3.7	48a	3.72
		48b	3.80

Figure 4

C_{36} 2+2 cycloadducts: (a) C_{18}+C_{18} (b) C_{16}+C_{20} (c) C_{14}+C_{22}

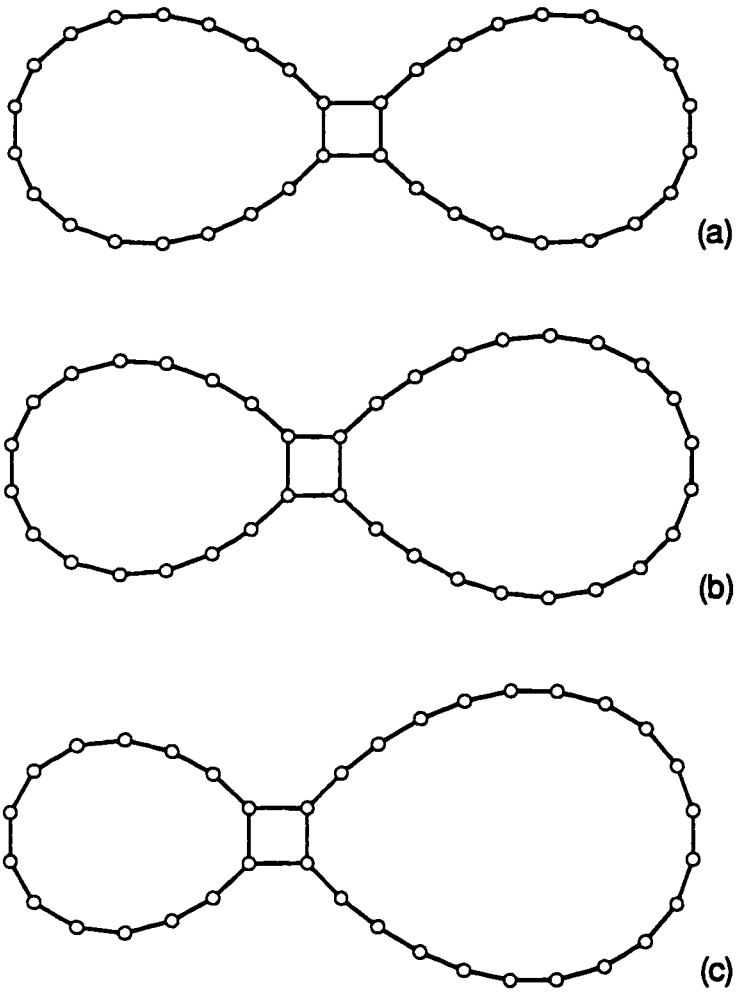

Table 3

Comparison of "Ring II" mobilities with calculated mobilities of 2+2 cycloadducts

(mobilities in cm^2/volt second)

Cluster size	Ring II Mobility	2+2 adduct	Mobility (calc)
C_{36}	3.30	18+18	3.29
		16+20	3.26
		14+22	3.25
C_{40}	2.92	20+20	2.92
		18+22	2.92
		16+24	2.91
C_{44}	2.7	22+22	2.64
		20+24	2.64
		18+26	2.63
C_{48}	2.45	24+24	2.39
		22+26	2.40
		20+28	2.39

Table 4

Comparison of "Ring III" mobilities with calculated mobilities of 2+4 cycloadducts

(mobilities in cm^2/volt second)

Cluster size	Ring III Mobility	2+4 adduct[a]	Mobility (calc)
C_{36}	3.70	18+18	3.64
		20+16	3.62
		16+20	3.65
C_{40}	3.26	20+20	3.26
		22+18	3.23
		18+22	3.20
C_{44}	2.95	22+22	2.87
		24+20	2.94
		20+24	2.92
C_{48}	2.7	24+24	2.66
		26+22	2.71
		22+26	2.63

[a]For asymmetric additions, the first ring listed contributes four atoms to the cycloaddition

Figure 5

Two perpendicular views of three C_{36} 2+4 cycloadducts: (a) C_{18}+C_{18} (b) C_{16}+C_{20}, where C_{20} contributes four atoms to the cycloaddition (c) C_{16}+C_{20}, where C_{16} contributes four atoms to the cycloaddition

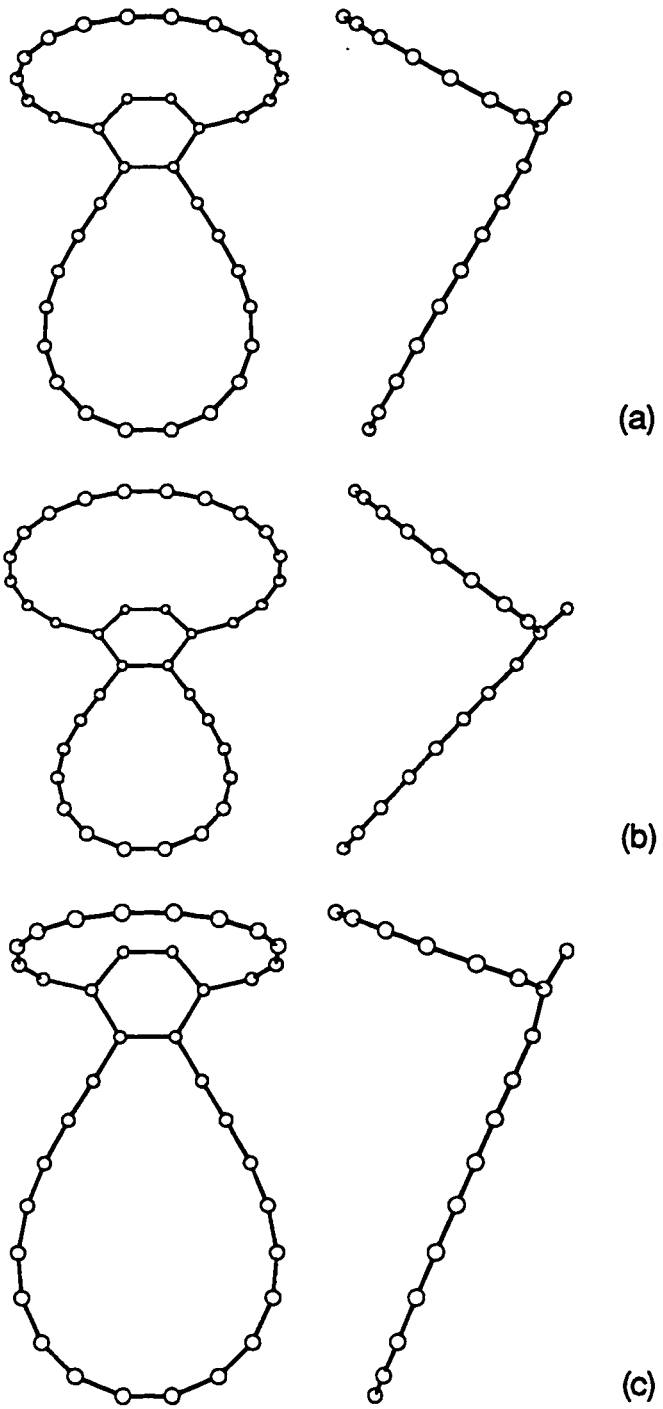

Table 5

Mobilities of 4+4 cycloadducts compared to Ring II results and 2+2 cycloadducts

(mobilities in cm^2/volt second)

Cluster size	Ring II	Adduct	4+4	2+2
C_{28}		14+14	4.70	4.24
C_{32}		14+18	4.01	3.69
C_{36}	3.30	18+18	3.47	3.29
C_{40}	2.92	22+18	3.04	2.92
C_{44}	2.7	22+22	2.76	2.64
C_{48}	2.45	26+22	2.47	2.40

Figure 6

Two perpendicular views of 4+4 cycloadducts:
(a) C_{28} (b) C_{32} (c) C_{36}

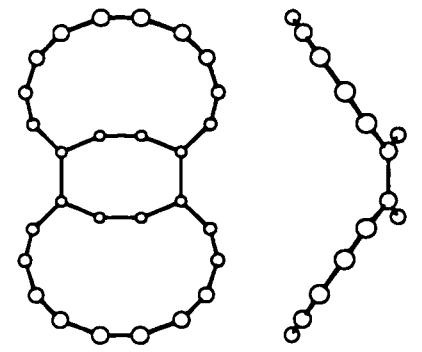

(a)

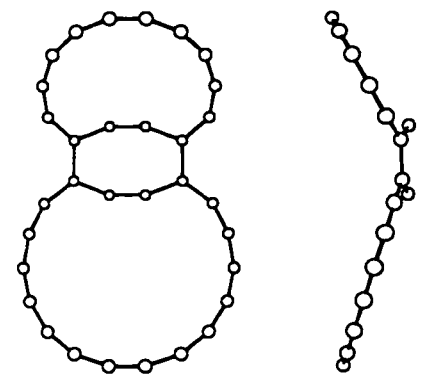

(b)

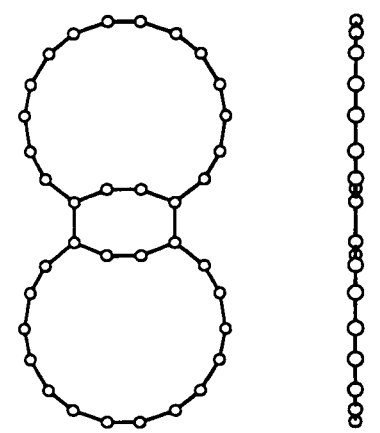

(c)

Table 6

Mobilities of 4+6 cycloadducts compared to Ring III results and 2+4 cycloadducts

(mobilities in cm^2/volt second)

Cluster size	Ring III	Adduct[a]	4+6	2+4
C_{36}	3.70	18+18	3.75	3.64
C_{40}	3.26	22+18	3.31	3.23
C_{44}	2.95	22+22	2.97	2.87
C_{48}	2.7	26+22	2.65	2.71

[a]For asymmetric additions, the ring listed first contributes the larger number of atoms to the cycloaddition.

Figure 7

Two perpendicular views of 4+6 cycloadducts: (a) C_{36} (b) C_{40} (c) C_{44}

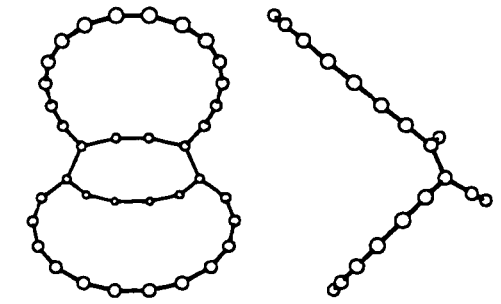

(a)

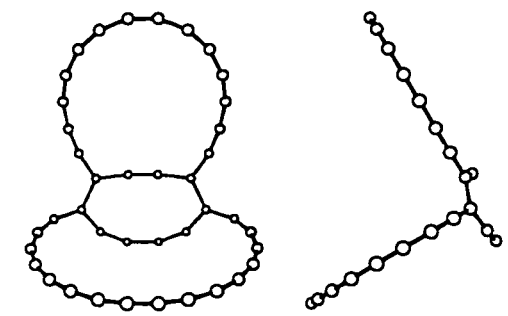

(b)

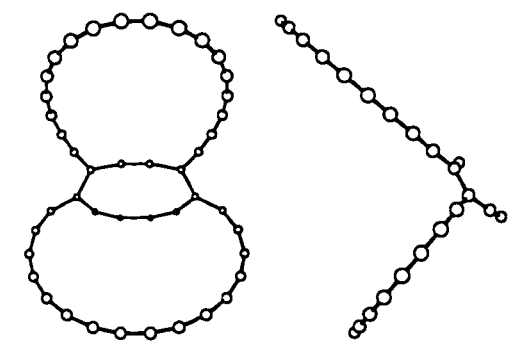

(c)

Chapter 3

The Case for 2+4 and 4+6 Cycloadducts

The mobility results establish the cycloadducts as **possibilities** for the clusters generated by graphite vaporization, but other questions remain. Why do 2+2 cycloadducts appear for cluster sizes throughout the twenties, whereas 2+4 cycloadducts are not seen until C_{30}? A plausible answer to that question will greatly support the cycloaddition model.

The question of whether or not a given cluster appears involves the energetics of the reaction that produces it. Detailed, accurate energies of reactants, products and transition states are needed, and for that high-level ab initio calculations are required. Geometries for the monocyclic rings, cycloadducts and transition structures are optimized with the Hartree-Fock (HF) method using a double zeta (DZ), or 4s2p, basis set formed by contracting the Huzinaga-Dunning[20] (9s5p) uncontracted Gaussian basis.

Energies at the DZ HF geometries are computed with the HF method using a double zeta plus polarization (DZP) basis, consisting of the DZ basis plus polarization function α_d=0.75. Also, the DZP basis is used for density functional theory (DFT) calculations. Two DFT methods are employed. One is a local density approximation (LDA) method which employs the Slater[21] exchange

---

[20]S. Huzinaga. *J. Chem. Phys.* **42**, 1293 (1965); T.H. Dunning, Jr. *J. Chem. Phys.* **53**, 2823 (1970).
[21]J.C. Slater. *Phys. Rev.* **81**, 385 (1951).

functional and the correlation functional of Vosko, Wilk, and Nusair.[22] The other employs the nonlocal (gradient-corrected) Becke[23] exchange functional and the nonlocal Perdew[24] correlation functional. This Becke-Perdew method is denoted BP. Hartree-Fock calculations are carried out by using the TURBOMOLE quantum chemistry package,[25] and DFT is introduced through a separate code[26] which interfaces with TURBOMOLE.

Density functional theory is implemented as a hybrid with Hartree-Fock, meaning that the exchange and correlation energies are computed using the Hartree-Fock electron density rather than a DFT density. The DFT total energies are computed by subtracting the HF exchange from the HF total energy and adding the DFT exchange and correlation energies. That is,

$$E^{DFT} = E^{HF} - E^{HF}_X + E^{DFT}_X + E^{DFT}_C$$

for a general DFT method, where E_X and E_C represent exchange and correlation energies, respectively. DZP BP should be considered the highest level of theory in this work, since it includes electron correlation whereas HF does not, and BP includes gradient corrections to the density, whereas LDA does not. HF and LDA calculations are included for comparison.

The particular clusters studied include monocyclic rings C_{10}, C_{14}, and C_{18}. These rings are chosen because they are Hückel 4n+2 rings. The cycloadducts selected are C_{20}, C_{24}, C_{28}, C_{32}, and C_{36}. This range of cycloadducts includes clusters on both sides of the appearance threshold for Ring III and should allow for a thorough exploration of the cycloaddition processes. 2+2, 2+4, and 4+6

---

[22]S.H. Vosko, L. Wilk, and M. Nusair. *Can. J. Phys.* **58**, 1200 (1980).
[23]A.D. Becke. *Phys. Rev. A* **38**, 3098 (1988).
[24]J.P. Perdew and Y. Wang. *Phys. Rev. B* **45**, 13244 (1992); J.P. Perdew, J.A. Chevary, S.H. Vosko, K.A. Jackson, D.J. Singh, and C. Fiolhais. *Phys. Rev. B* **46**, 6671 (1992).
[25]R. Ahlrichs, M. Bär, M. Häser, H. Horn, and C. Kölmel. *Chem. Phys. Lett.* **162**,165 (1989).
[26]G.K. Odom and G.E. Scuseria (unpublished results).

cycloaddition energetics are quantified using the theoretical methods outlined above. The DZ HF ground states for 2+4 and 4+6 adducts and their transition states are electronic singlets. Transition states for 2+2 adducts have triplet electronic configurations, and the 2+2 adducts themselves are predicted by DZ HF to have triplet ground states. However, DZP BP predicts singlet states for the 2+2 adducts, and the results reported in this work are for singlet 2+2 cycloadducts.

The first question to be answered by these calculations is whether the transition barriers for 2+2, 2+4, and 4+6 cycloaddition are a function of cluster size over the range of 20-36 atoms. If the barriers to 2+4 and 4+6 are appreciably higher for sizes below C_{30} than above C_{30}, then the appearance threshold for Ring III can be explained simply as a result of prohibitively high reaction barriers below the threshold.

DZP BP results are shown in Table 7 and do not show the radical changes in energy required to explain the appearance thresholds. The 2+2 barriers are within a few tenths of an eV of each other over the range 20-36 atoms (a tenth of an eV is 2.3 kcal/mol), which is consistent with experiment because 2+2 adducts are observed throughout the size regime considered. However, 2+4 and 4+6 barriers across the C_{30} threshold also do not vary by more than a few tenths of an eV. Further, while LDA barriers tend to be quantitatively lower than the barriers for HF or BP, both LDA and HF give barriers that follow the qualitative trends shown by BP. The DZP BP barriers do not support any kind of assertion that 2+4 of 4+6 cycloadducts should form selectively at sizes above C_{30}. At first glance, this would appear to present a problem for the cycloaddition model.

However, under the Woodward-Hoffmann rules for cycloaddition processes, the symmetry rules that permit a cycloaddition to occur also permit

the reverse process under the same conditions. A cycloaddition may occur and be immediately followed by the corresponding retrocycloaddition. This makes it important to determine ΔE for the cycloaddition processes because the reverse barrier equals the forward barrier minus ΔE.

The DZP BP ΔE data for the cycloadducts are shown in Table 9, and these data provide a clear explanation for the observed appearance thresholds. The 2+2 cycloadditions are exothermic by more than 2 eV (nearly 50 kcal/mol) over the entire range from 20-36 atoms. Once formed, a 2+2 cycloadduct would be very stable and tend not to dissociate. For larger clusters, such as C_{32} and C_{36}, the 2+4 and 4+6 cycloadducts have stability similar to the 2+2 adducts. However, for the smaller clusters, the 2+4 and 4+6 cycloadducts are much less stable and may dissociate back to their constituent monocyclic rings. This is the explanation that demonstrates that 2+4 and 4+6 cycloaddition are consistent with experimental observations about Ring III.

If resistance to retrocycloaddition is the key to whether a given cycloadduct will be experimentally observed, then the DZP BP level of theory can be used to establish an empirical rule that a cycloaddition process must be exothermic by more than 2 eV to produce an adduct that resists dissociation. This rule would predict 2+2 adducts at all sizes from 20-36 atoms and 2+4 and 4+6 adducts at sizes with more than 30 atoms, which is consistent with the experimental observations. This rule is qualitative in nature and only applies to the DZP BP level of theory, and there certainly exists no physical reason why 2 eV should be the threshold. Higher levels of theory, such as coupled-cluster theory (as CCSD or CCSD(T)), could reflect the same behavioral trends as DZP BP and perhaps show a threshold of 1 eV or 3 eV or something else entirely.

The "2 eV rule" is simply a guideline for evaluating the DZP BP results in this work.

As for the large 4+4 cycloadducts which were shown in Chapter 2 to have Ring II mobilities, the "2 eV rule" can be used to evaluate them as candidates for Ring II. DZ HF optimizations have been performed on C_{44} 2+2 and 4+4 cycloadducts formed from two C_{22} rings. Triplet state results for the 4+4 adduct are reported because both DZ HF and DZP BP predict a triplet ground state. DZP BP calculations at these DZ HF geometries give ΔE results of -1.89 eV for 4+4 cycloaddition and -2.10 eV for 2+2 cycloaddition. The 2+2 cycloadduct passes the "2 eV test" whereas the 4+4 adduct does not, so the 4+4 cycloadduct is at best a marginal candidate for Ring II. Therefore, the Ring II peak at C_{44} is very likely caused by 2+2 adducts, and it is unlikely that 4+4 adducts are being observed even at cluster sizes for which 4+4 mobilities are experimentally consistent.

The DZP HF and DZP LDA data in Table 10 support the BP trends, with LDA predicting greater exothermicities than either HF or BP. However, LDA is known to overestimate bond strengths, so the BP results are likely the most accurate. All three levels of theory predict that 2+4 and 4+6 cycloadditions are more exothermic for larger clusters than for smaller clusters.

The cycloaddition model, therefore, is consistent with two important experimental observations. First, the cycloadducts have been shown to have cluster mobilities that match the mobilities observed in the ion chromatography experiments. Also, the energetics of the cycloaddition reactions provide a clear and simple explanation for the observed cluster appearance thresholds. The cycloaddition model provides a complete and plausible interpretation of the graphite ion chromatography experiments.

Table 7

DZP BP barriers to cycloaddition processes
(barriers in eV)

Process	C_{20} 10+10	C_{24} 10+14	C_{28} 14+14	C_{32} 14+18	C_{36} 18+18
2+2	2.38	2.66	2.06	2.69	1.91
2+4	1.61	1.27	1.05	0.90	0.93
4+6		1.80	1.38	1.33	0.91

Table 8

DZP HF and DZP LDA barriers to cycloaddition processes
(barriers in eV)

DZP HF

Process	C_{20} 10+10	C_{24} 10+14	C_{28} 14+14	C_{32} 14+18	C_{36} 18+18
2+2	3.50	2.90	3.14	1.90	3.27
2+4	3.40	2.62	2.06	2.10	2.24
4+6		2.70	1.90	2.11	1.28

DZP LDA

Process	C_{20} 10+10	C_{24} 10+14	C_{28} 14+14	C_{32} 14+18	C_{36} 18+18
2+2	1.77	2.33	1.89	2.74	1.69
2+4	0.52	0.32	0.22	0.02	0.03
4+6		0.89	0.63	0.63	0.29

Table 9

DZP BP ΔE for cycloaddition processes
(energies in eV)

Process	C_{20} 10+10	C_{24} 10+14	C_{28} 14+14	C_{32} 14+18	C_{36} 18+18
2+2	-2.35	-2.46	-2.51	-2.46	-2.42
2+4	-0.24	-1.26	-1.73	-2.10	-2.20
4+6	-0.59	-1.29	-1.81	-2.21	-2.25

Table 10

DZP HF and DZP LDA ΔE for cycloaddition processes
(energies in eV)

DZP HF

Process	C_{20} 10+10	C_{24} 10+14	C_{28} 14+14	C_{32} 14+18	C_{36} 18+18
2+2	-2.15	-2.48	-2.80	-2.60	-2.41
2+4	-0.29	-1.55	-1.96	-2.23	-2.04
4+6	-0.16	-1.81	-2.11	-2.57	-2.28

DZP LDA

Process	C_{20} 10+10	C_{24} 10+14	C_{28} 14+14	C_{32} 14+18	C_{36} 18+18
2+2	-3.44	-3.44	-3.36	-3.32	-3.28
2+4	-1.64	-2.58	-2.98	-3.37	-3.49
4+6	-2.22	-2.78	-3.20	-3.61	-3.66

Chapter 4

From Cycloadducts to Rings and "Hoops"

What happens to the cycloadducts after they are formed? It has been suggested previously[27] that 2+2 cycloadducts can transform to fullerenes, but this seems unlikely because 2+2 adducts with 20-30 carbon atoms fail to produce fullerenes despite strong theoretical evidence[28] that fullerenes are much more stable than carbon rings that are seen in this size range. However, a 2+2 cycloadduct can undergo a 2+2 retrocycloaddition process which breaks two bonds to form a single large monocyclic ring. The newly formed large ring can react to form still larger cycloadducts. Larger 2+2 cycloadducts can react to form larger rings, and so on. Rings with as many as 60 atoms have been detected by ion chromatography techniques.[27]

2+4 and 4+6 cycloadducts have no such reaction that leads to a larger ring. However, these clusters can, with a modest barrier, undergo cyclization reactions around the site of the initial cycloaddition. In the present model, the cycloadduct undergoes a sequence of cyclizations that results in a cylindrical carbon species that is denoted here as a carbon "hoop." For a C_{36} 2+4 cycloadduct of two C_{18} carbon rings, the transformation to a hoop has been mapped out using the semiempirical TB method. TB optimized structures for the

---

[27]J.M. Hunter, J.L. Fye, E.J. Roskamp, and M.F. Jarrold. *J. Phys. Chem.* **98**, 1810 (1994).
[28]P.R. Taylor, E. Bylaska, J.H. Weare, and R. Kawai. *Chem. Phys. Lett.* **235**, 558 (1995).

minima along the path are shown in Figure 8, and the TB energetics are presented in Table 11. At the TB level of theory, each step in the hoop formation is exothermic and has a modest barrier. The overall process is exothermic by more than 2.5 eV. A similar hoop assembly exists for the C_{36} 4+6 cycloadduct. The minima are pictured in Figure 9, and detailed TB energetics are given in Table 12. The resultant hoop is identical to the one formed from the 2+4 adduct. Both cycloadducts are viable starting materials for hoop formation.

Do these results hold up at higher levels of theory? DZ HF optimizations have not been carried out at each step of hoop formation because of the expense of optimizing in C_1 symmetry (that is, no symmetry) and the difficulty of finding transition states in C_1 symmetry without analytic second derivatives. However, DZ HF optimizations have been performed out on a sequence of the hoops themselves. Using these DZ HF geometries, DZP HF, DZP LDA, and DZP BP energies have been computed for hoops with sizes ranging from 28 to 60 atoms. The DZP BP energetics are detailed in Table 13. This data illustrates that, as cluster size increases, hoops become increasingly stable with respect to monocyclic precursors.

For the hoops, the HF and LDA results diverge wildly from BP, as illustrated in Table 14. The LDA results predict hoops to have far greater stability than BP with respect to monocyclic rings. This is a clear demonstration of the tendency of LDA to overestimate bond energies. HF theory predicts that hoops are actually less stable than the constituent carbon rings. The HF method underestimates bond energies, which disfavors the hoops because the angle strain of the triple bonds outweighs the stability conferred by the additional bonds.

The highest level of theory in this work, DZP BP energies at DZ HF geometries, predicts that the transformation from cycloadducts to hoops is energetically favorable for all cluster sizes for which the Ring III species are observed experimentally. This mechanism also provides an explanation for the McElvany ring addition results in which, for example, laser desorption of C_{18} rings results in a series of C_{18n} products. The process is not constrained to use only two rings. The hoop itself contains many sites suitable for further cycloaddition should it collide with another ring. Figure 10 illustrates an example, a 2+4 cycloadduct between a C_{18} ring and the C_{36} hoop. This adduct is a C_{54} object which could react with another ring, and so on, to form other cylindrical clusters. The pathway from cycloadducts to hoops introduces a significant amount of graphitic (sp^2) character to the carbon clusters. Can a hoop become a fullerene, which is an all-sp^2 molecule?

Figure 8

Minima along the path from C_{18}+C_{18} 2+4 cycloadduct to C_{36} hoop

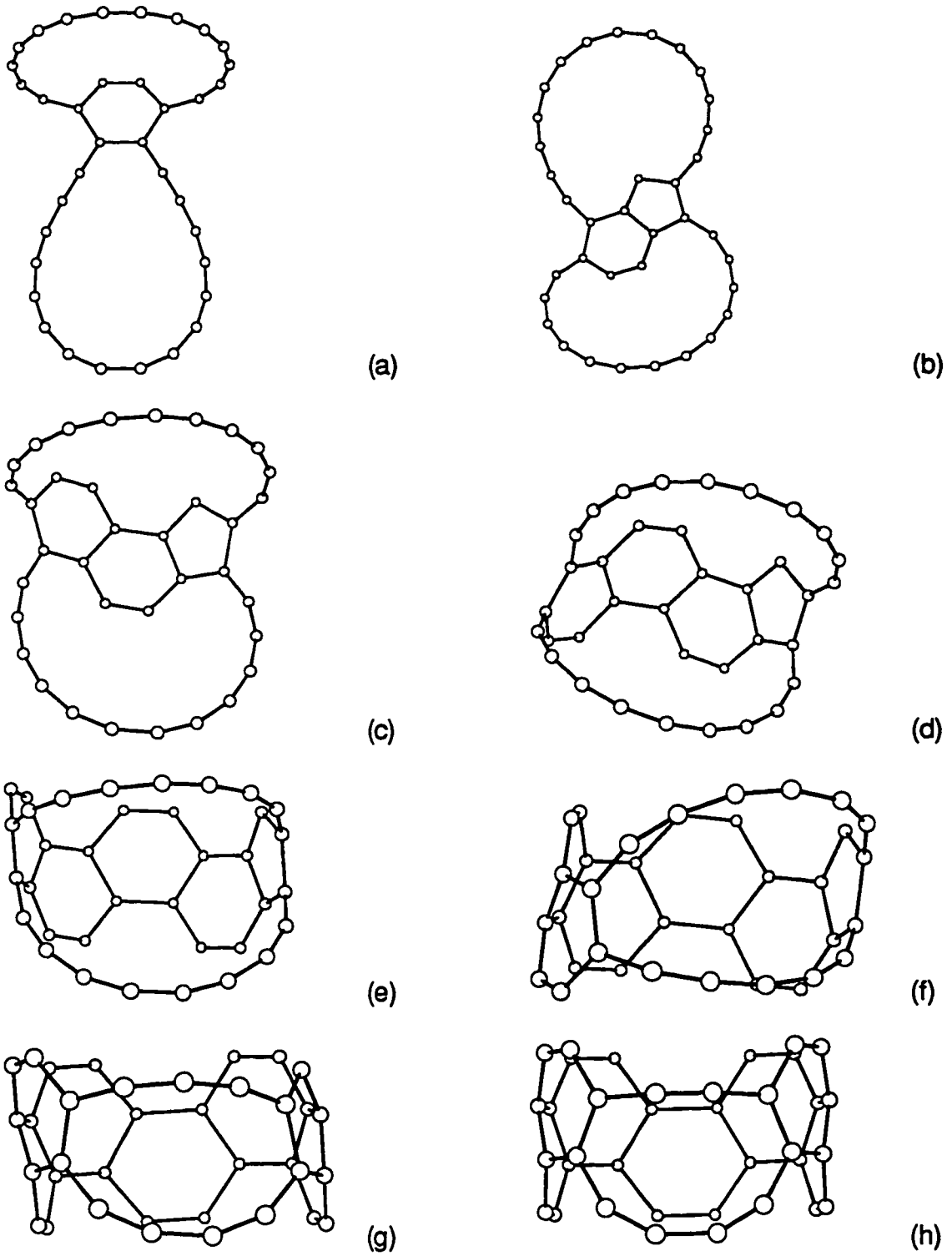

Table 11

TB energetics of pathway from 2+4 cycloadduct to C_{36} hoop as shown in Figure 8

(relative energies in eV)

Step	E(minima)	E(t.s.)
(a, adduct)	0.00	
		+0.87
(b)	-0.29	
		+0.87
(c)	-0.51	
		+0.61
(d)	-0.85	
		+0.16
(e)	-1.09	
		-0.14
(f)	-1.47	
		-0.47
(g)	-1.53	
		-0.54
(h, hoop)	-2.66	

Figure 9

Minima along the path from C_{18}+C_{18} 4+6 cycloadduct to C_{36} hoop

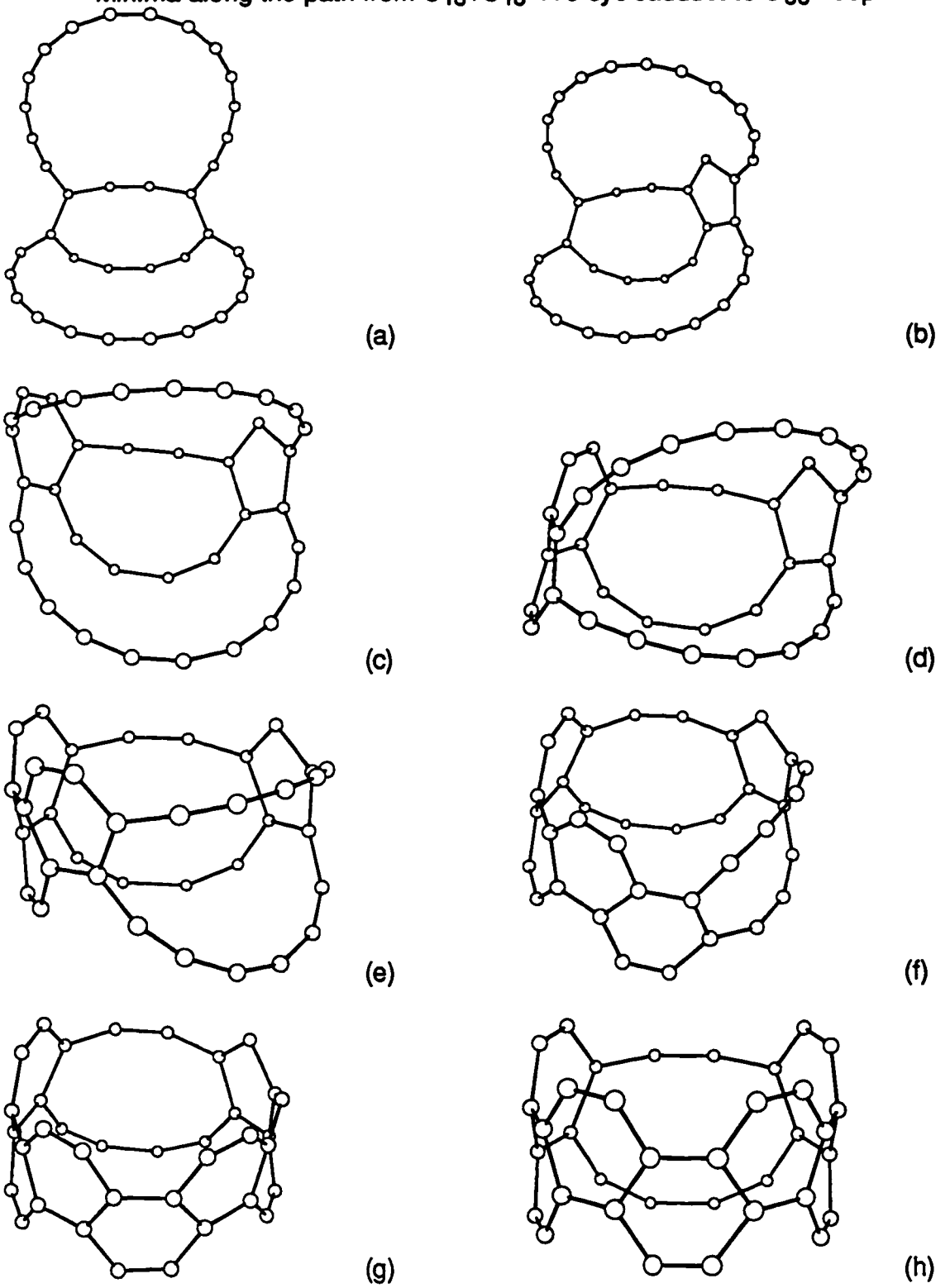

Table 12

TB energetics of pathway from 4+6 cycloadduct to C_{36} hoop as shown in Figure 9

(relative energies in eV)

Step	E(minima)	E(t.s.)
(a, adduct)	0.00	
		+0.90
(b)	-0.23	
		+0.73
(c)	-0.56	
		+0.47
(d)	-0.90	
		+0.03
(e)	-1.18	
		-0.21
(f)	-1.38	
		-0.21
(g)	-0.86	
		-0.22
(h, hoop)	-2.61	

Table 13

DZP BP energies of carbon hoops relative to monocyclic precursors

(energies in eV)

Hoop size	Rings	Energy
C_{28}	14+14	-2.03
C_{32}	14+18	-2.45
C_{36}	18+18	-3.28
C_{40}	18+22	-3.80
C_{44}	22+22	-4.05
C_{48}	22+26	-4.21
C_{52}	26+26	-4.70
C_{56}	26+30	-5.24
C_{60}	30+30	-5.32

Table 14

DZP HF and DZP LDA energies of carbon hoops relative to monocyclic precursors

(energies in eV)

Hoop size	Rings	HF energy	LDA energy
C_{28}	14+14	+0.68	-5.76
C_{32}	14+18	+2.12	-7.38
C_{36}	18+18	+1.13	-8.19
C_{40}	18+22	+2.35	-9.90
C_{44}	22+22	+1.80	-10.18
C_{48}	22+26	+3.26	-11.46
C_{52}	26+26	+2.38	-12.02
C_{56}	26+30	+3.54	-13.72
C_{60}	30+30	+3.04	-13.77

Figure 10

C_{54} 2+4 cycloadduct between C_{36} hoop
and C_{18} monocyclic ring

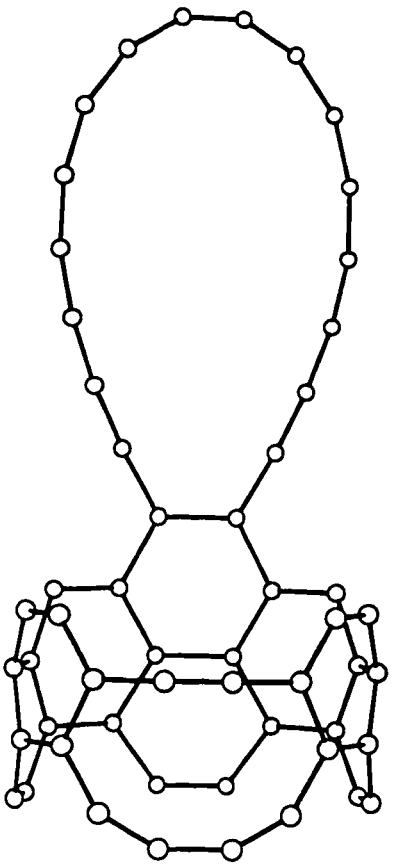

Chapter 5

1,2-carbon shifts

Carbon hoops have a large number of triple bonds between atoms whose bond angles are not 180°. The bond angle strain should make those sites very susceptible to reactions which rearrange the bonds. One such reaction is the 1,2-carbon shift. In a 1,2-carbon shift, a hexagon becomes a pentagon with a dangling atom attached, as illustrated in Figure 11. After two 1,2-shifts have occurred on neighboring triple bonds, the two dangling atoms can bond to each other to form a new pentagon or hexagon. In this way, a hoop can close its top and bottom faces with new polygons and thereby form a spherical cage.

Energetics of 1,2-carbon shifts have been explored with the DZP HF, DZP LDA and DZP BP methods on DZ HF optimized geometries. Calculations are first performed on small model systems which simulate a section of a hoop, as shown in Figure 12. For these systems, which have hydrogen atoms replacing the connections to the rest of the hoop, minima and transition states have been optimized. The DZP BP energetics are presented in Table 15. For actual hoops, minima have been optimized for C_{32}, C_{36}, and C_{40}, and the energetics are also shown in Table 15.

The DZP BP data indicate that the transition barriers for 1,2-shifts on the model systems are 1.67 and 1.92 eV. ΔE for small systems are between +1.1 and +1.3 eV. ΔE results for the carbon hoops qualitatively follow the data for the

small molecules, and it is assumed that the transition barriers for the hoops similarly follow. The best results in this study indicate that a 1,2-shift occurs with a barrier of less than 2 eV.

Transition barriers of 2 eV and ΔE around 1.3 eV require that the hoop put approximately 3.3 eV into the 1,2-shift process before any energy can be recovered. That is the energy to perform two 1,2-carbon shifts. After the first two shifts, the first new polygon forms, and the electronic energy of the cluster drops significantly, which fuels further carbon shifts. These new carbon shifts form more polygons, which liberates more energy for more reactions. The process continues until cage closure occurs, with a very large total drop in the cluster's electronic energy.

For the C_{36} hoop discussed in the previous chapter, the path from hoop to initial cage closure has been mapped using the semiempirical TB method. Minima and transition states are optimized, and the TB energetic data are shown in Table 16. Minima along the path are illustrated in Figure 13. The total process lowers the electronic energy of the cluster by 10.6 eV. However, it is interesting to note that the initial cage is not the D_{2d} isomer which is known to be most stable. The cage still must find a way to its most stable form.

Figure 11

1,2-carbon shift

Reactant

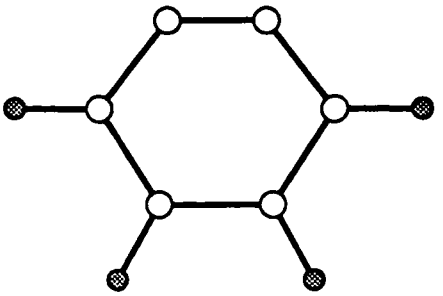

Product

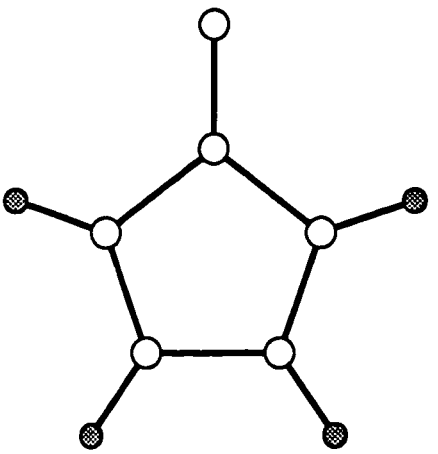

Figure 12

1,2-carbon shifts on model systems

$C_{14}H_4$ reactant

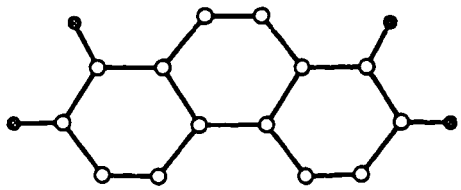

$C_{14}H_4$ product

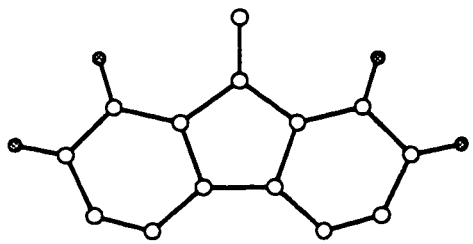

$C_{22}H_4$ reactant

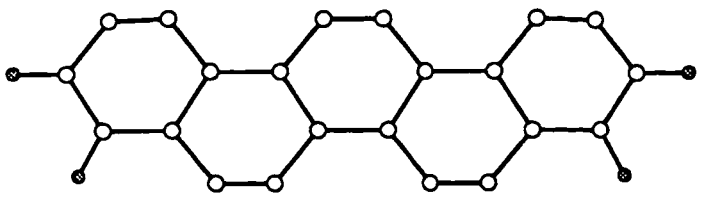

$C_{22}H_4$ product

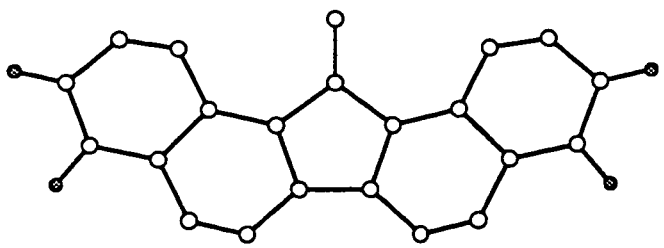

Table 15

DZP BP energetics of 1,2-carbon shifts

(energies in eV)

Molecule	Barrier	ΔE
$C_{14}H_4$	+1.67	+1.15
$C_{22}H_4$	+1.92	+1.28
C_{32} hoop		+1.91
C_{36} hoop		+1.33
C_{40} hoop		+1.69

Figure 13

Pathway from C_{36} hoop to a closed cage
(continues on following page)

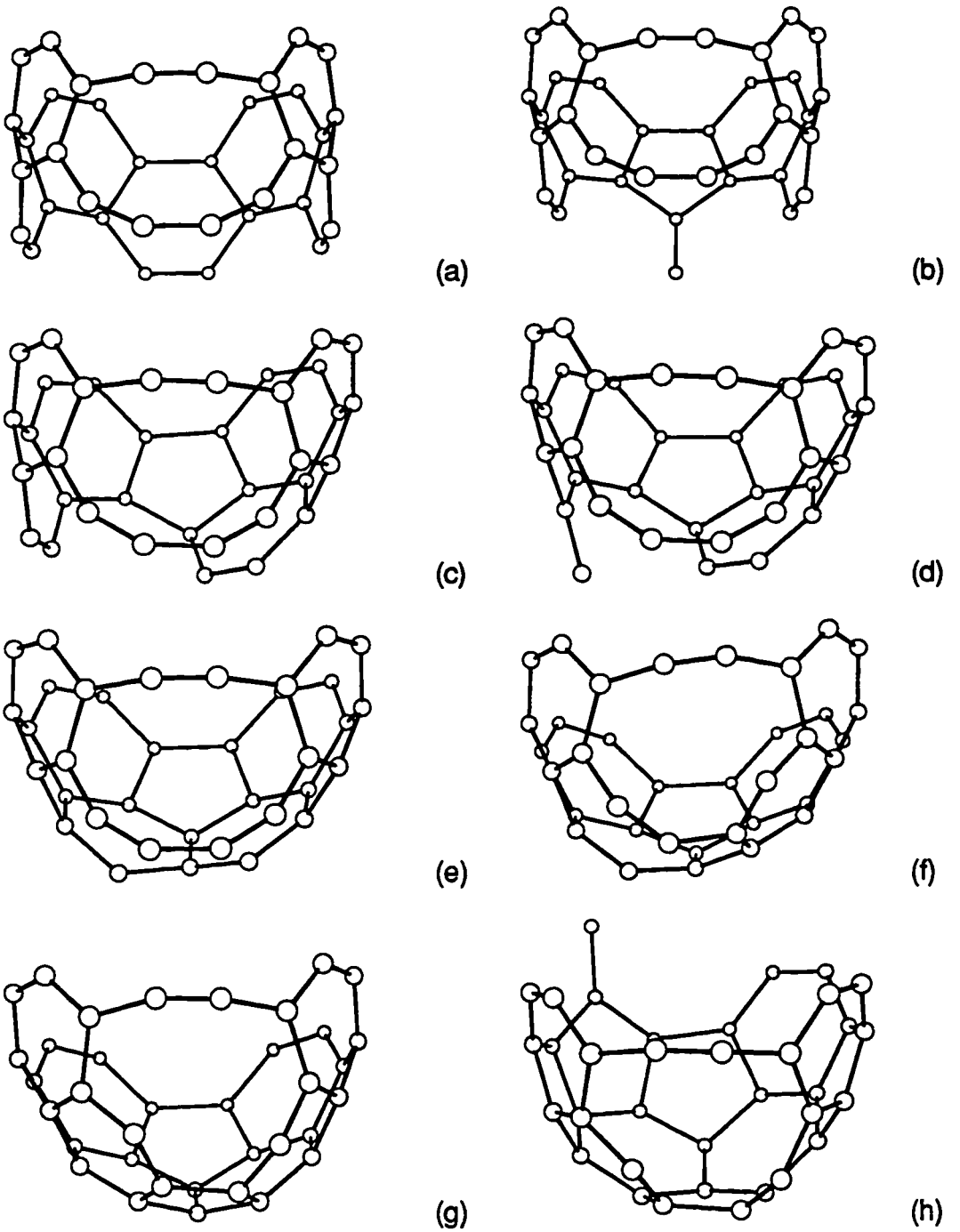

Figure 13
(continued from previous page)

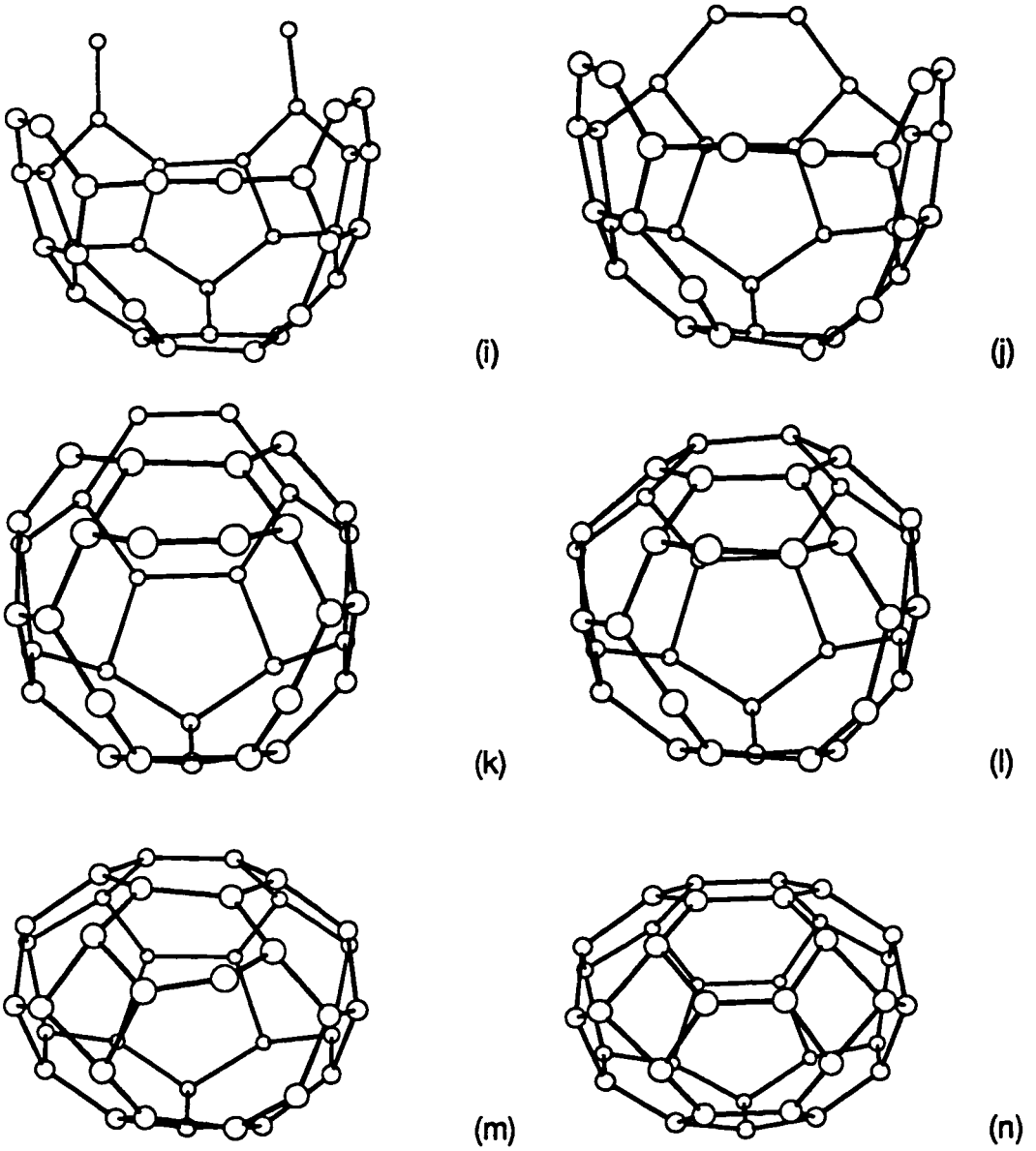

Table 16

TB energetics for pathway from C_{36} hoop to a closed cage as shown in Figure 12

(energies in eV)

Step	E(minima)	E(t.s.)
(a, hoop)	0.00	
		+2.42
(b)	+1.21	
		+3.83
(c)	-1.53	
		+0.69
(d)	-0.56	
		-0.56
(e)	-2.32	
		-2.16
(f)	-4.12	
		-4.12
(g)	-6.39	
		-3.00
(h)	-4.14	
		-0.92
(i)	-2.11	
		-1.92
(j)	-5.77	
		-3.59
(k)	-3.88	
		-3.44
(l)	-9.54	
		-8.88
(m)	-8.90	
		-8.80
(n)	-10.57	

Chapter 6

Annealing and Fragmentation

Once the carbon cage is closed, there is no guarantee that the cage will be the most stable isomer for the particular fullerene. In fact, it is highly improbable that the fullerene generation experiments would yield the most stable isomer of any fullerene upon initial cage closure. However, the cages can isomerize by undergoing processes that rearrange the polygons composing the cage. Such reactions are collectively referred to as annealing processes.

The best known annealing process is the Stone-Wales,[29] or pyracylene, rearrangement. Two pentagons and two hexagons exchange places in a section of a fullerene surface, as illustrated in Figure 14. The Stone-Wales reaction on the buckminsterfullerene molecule has been characterized by theoretical means.[30] A more general class of Stone-Wales type reactions, in which a C_2 bond rotates 90° irrespective of the number of atoms in the surrounding polygons, has also been studied.[31] Both Stone-Wales studies employed the semiempirical MNDO method, as well as HF and DFT methods.

Results from these studies predict that the barrier to Stone-Wales type rearrangements is, in general, about 6-7 eV, which is the highest barrier of any reaction in the present fullerene assembly model. However, by the time cage

---

[29]A.J. Stone and D.J. Wales. *Chem. Phys. Lett.* **128**, 501 (1986).
[30]R.L. Murry, D.L. Strout, G.K. Odom, and G.E. Scuseria. *Nature* **366**, 665 (1993).
[31]R.L. Murry, D.L. Strout, and G.E. Scuseria. *Int. J. Mass Spectrom. Ion Proc.* **138**, 113 (1994).

closure occurs, an enormous lowering of the electronic energy of the cluster has taken place, with a corresponding conversion of that energy to vibration. This vibrational energy is the means whereby the annealing barriers can be overcome. To illustrate the magnitude of the lowering of the electronic energy, DZP BP calculations have been performed on several fullerenes, with comparison to the energies of the original monocyclic rings, and the results are shown in Table 17. Since fullerenes are more stable than monocyclic rings by 20 eV and more, overcoming the barriers to Stone-Wales type rearrangements is not a problem. Therefore, cages that form from the hoops are able to isomerize to find the most stable structure. TB energetics for a complete path from rings to the most stable fullerene are shown for C_{36} and C_{60} in Figures 15 and 16, respectively.

However, the vast release of energy resulting from cage formation can also cause the fullerenes to fragment. It is known[32] that fullerenes fragment by ejecting C_2 radicals, and if enough energy is input, a fullerene can be fragmented down to size C_{32}, at which point the cage tears itself apart rather than lose another C_2. Fragmentation of buckminsterfullerene has been studied[30] by theoretical means and found to require about 12 eV of energy. It has also been observed[1] that, in the graphite vaporization experiment, the more the carbon clusters are allowed to "cook," the more C_{60} BF dominates the mass spectrum. "Cooking" refers to annealing and fragmentation processes whereby clusters can use their tremendous store of vibrational energy to sample the potential energy surface in search of stable structures. Fullerenes larger than C_{60} can fragment to form 60-atom cages and then anneal to find the buckminsterfullerene structure. Fullerenes smaller than C_{60} can either collide with other clusters to

---

[32]S.C. O'Brien, J.R. Heath, R.F. Curl, and R.E. Smalley. *J. Chem. Phys.* **88**, 220 (1988).

form molecules with more than sixty atoms or fragment to the point where they shatter completely. C_{60}, and to a lesser degree C_{70}, become prominent because of their thermodynamic stability.[31] This is how C_{60} and C_{70} dominate fullerene generation experiments.

Figure 14

Stone-Wales rotation: (a) reactant (b1) transition state for planar pathway (b2) transition state for sp^3 pathway, ref. 30 (c) product

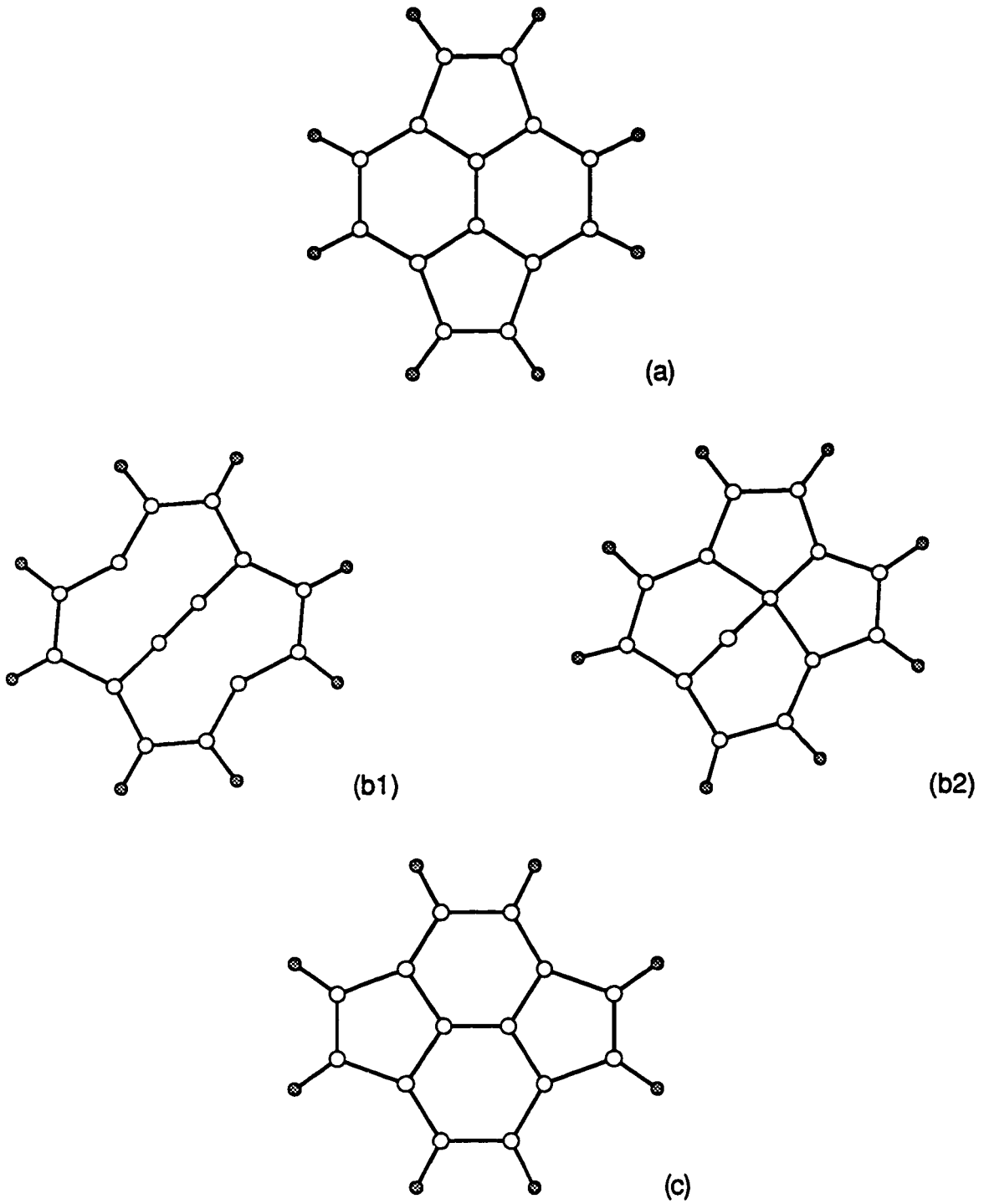

Table 17

DZP BP energies of fullerenes relative to monocyclic precursors

(energies in eV)

Fullerene	Rings	Rel. energy
C_{32}	14+18	-18.86
C_{36}	18+18	-21.86
C_{40}	18+22	-25.88
C_{44}	22+22	-30.29
⋮		
C_{60}	30+30	-50.13

Figure 15

TB energetics for a path from two C_{18} rings to the most stable C_{36} fullerene (minima are represented by diamonds; transition states by crosses)

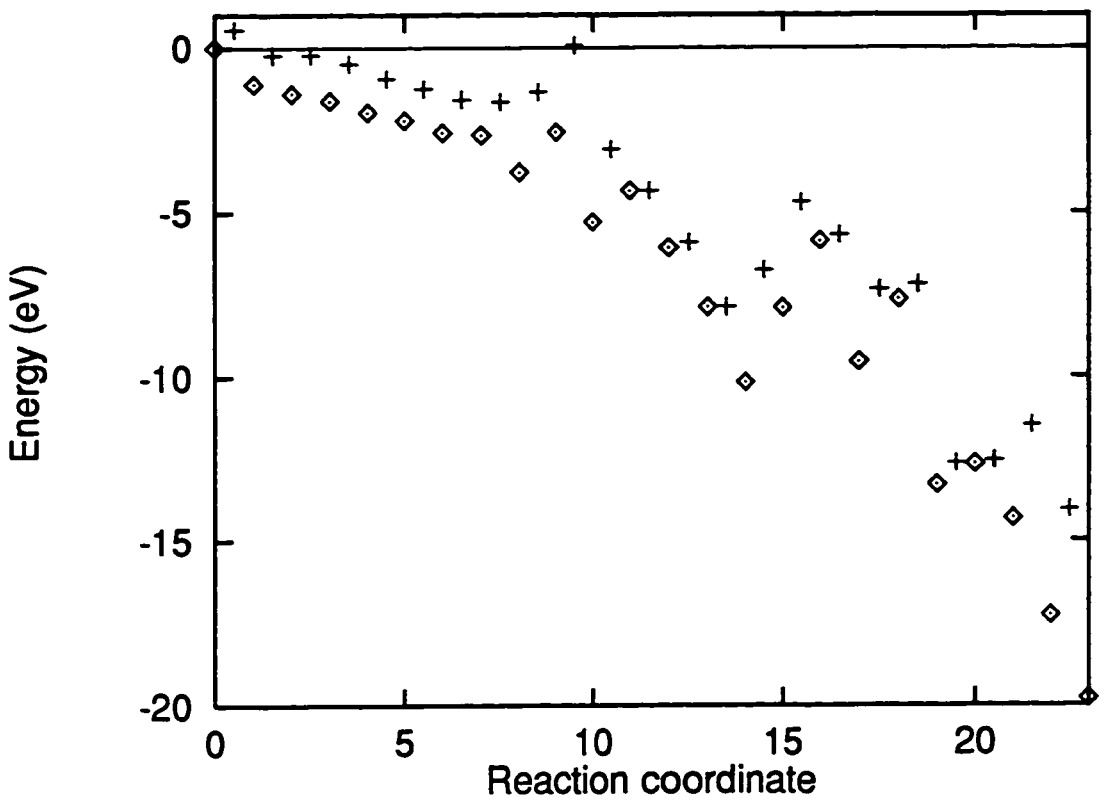

Figure 16

TB energetics for a path from two C_{30} rings to C_{60} buckminsterfullerene (minima only, represented by diamonds)

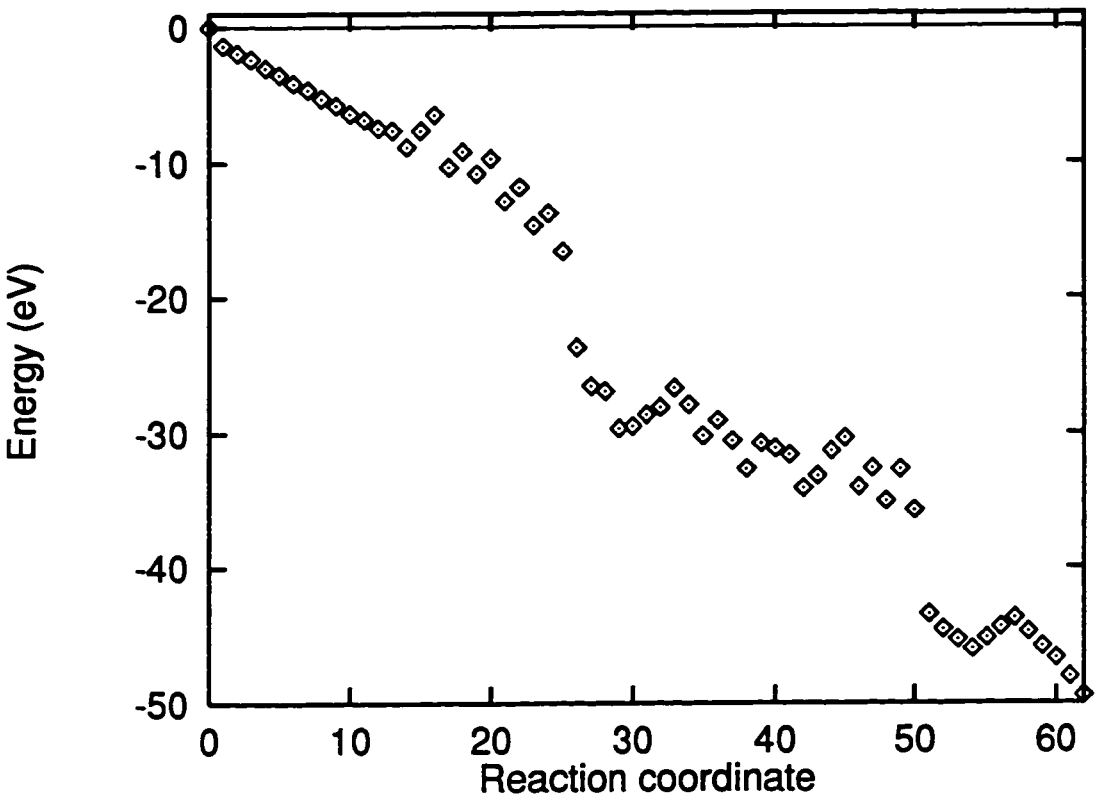

Chapter 7

Conclusion

The cycloaddition model provides a complete, explicit pathway from monocyclic carbon rings to fullerenes. This model is consistent with current experimental results and elucidates the road to fullerenes with energetic information obtained at high levels of theory. Also, this model is simply a path to closure of a carbon cage, any cage, rather than relying on contrived mechanisms which are directed toward specific cages. Annealing and fragmentation are all that is required to bring buckminsterfullerene to prominence. These are the advantages of the model.

In the cycloaddition model, experimentally observed monocyclic rings collide to create a variety of cycloadducts. The appearance of 2+2, 2+4, and 4+6 cycloadducts can be supported by experimental data. 2+2 adducts open via a retro-2+2 process to form larger monocyclic rings, which could be called "second generation" rings. Second generation rings collide with other rings to form large cycloadducts. Large 2+2 cycloadducts can open to form third generation rings, and so on.

2+4 and 4+6 cycloadducts do not have a low-energy path to second generation monocyclic rings. Rather, they undergo a series of cyclizations to form carbon hoops. Carbon hoops undergo 1,2-carbon shifts and further cyclizations to generate closed cages. These cages anneal to find the most

stable isomer. The elements of the cycloaddition model are represented graphically in Figure 17.

The model appears to resemble the "fullerene road" in that a wide variety of fullerenes anneal and fragment to form buckminsterfullerene in abundance. However, the cycloaddition model provides important details as to how these fullerenes are formed in the first place. Moreover, the model does not rely on the substantial quantities of C_2 which are required by the fullerene road. The cycloaddition model also has important differences from the so-called "ring stacking" models. While both rely on reactions between carbon rings, the cycloaddition model is not only more explicit about chemical detail but also demonstrates fullerene formation with as few as two rings. Also, the model is shown to be general, explaining the formation of fullerenes with fewer than 60 atoms as well as those with more than 60 atoms.

The cycloaddition model and the "pentagon road" appear to share no essential common features, and it has been noted that the curved graphitic sheets in the pentagon road model are not observed in the ion chromatography experiments. However, the lack of "open fullerenes" in the experiments is not a valid indictment of the pentagon road. Fullerene formation is clearly a complex process that requires many steps and has many reaction intermediates. These intermediates represent a wide range of stages along the path to fullerenes, and the carbon clusters should not show large changes in mobility from one reaction step to the next. Therefore, if every intermediate were observed, the arrival time distribution for any cluster size above C_{30} would show a continuum of highly overlapping peaks with little hope of resolution. Neither the pentagon road nor the cycloaddition model is dependent upon the observation of all intermediates. However, the ion chromatography experiments provide explicit support for the

cycloaddition model whereas they do not provide evidence for or against the pentagon road.

The cycloaddition model is a useful tool for understanding fullerene formation. Reaction pathways in this model are both consistent with experimental observations and plausible from a computational point of view. A new interpretation of the graphite vaporization ion chromatography results is developed into a fullerene assembly model based on reactions which are shown by theoretical calculations to have reasonable energetics. This cycloaddition model is a novel, successful approach toward the elucidation of the fullerene formation process.

Figure 17

The cycloaddition model for fullerene formation